

Explicitly modelled deep-time tidal dissipation and its implication for Lunar history

Green, Mattias; Huber, Matthew; Waltham, David; Buzan, Jonathan; Wells, Martin

Earth and Planetary Science Letters

DOI:

[10.1016/j.epsl.2016.12.038](https://doi.org/10.1016/j.epsl.2016.12.038)

Published: 01/03/2017

Peer reviewed version

[Cyswllt i'r cyhoeddiad / Link to publication](#)

Dyfyniad o'r fersiwn a gyhoeddwyd / Citation for published version (APA):

Green, M., Huber, M., Waltham, D., Buzan, J., & Wells, M. (2017). Explicitly modelled deep-time tidal dissipation and its implication for Lunar history. *Earth and Planetary Science Letters*, 461, 46–53. <https://doi.org/10.1016/j.epsl.2016.12.038>

Hawliau Cyffredinol / General rights

Copyright and moral rights for the publications made accessible in the public portal are retained by the authors and/or other copyright owners and it is a condition of accessing publications that users recognise and abide by the legal requirements associated with these rights.

- Users may download and print one copy of any publication from the public portal for the purpose of private study or research.
- You may not further distribute the material or use it for any profit-making activity or commercial gain
- You may freely distribute the URL identifying the publication in the public portal ?

Take down policy

If you believe that this document breaches copyright please contact us providing details, and we will remove access to the work immediately and investigate your claim.

Explicitly modelled deep-time tidal dissipation and its implication for Lunar history

J.A.M Green^{a,*}, M. Huber^b, D. Waltham^c, J. Buzan^b, M. Wells^d

^a*School of Ocean Sciences, Bangor University, Menai Bridge, United Kingdom*

^b*Department of the Earth Sciences, The University of New Hampshire, Durham, New Hampshire, USA*

^c*Department of Earth Sciences, Royal Holloway University of London, Egham, United Kingdom*

^d*Department of Earth Science & Engineering, Imperial College London, London, United Kingdom*

Abstract

Dissipation of tidal energy causes the Moon to recede from the Earth. The currently measured rate of recession implies that the age of the Lunar orbit is 1500 My old, but the Moon is known to be 4500 My old. Consequently, it has been proposed that tidal energy dissipation was weaker in the Earth's past, but explicit numerical calculations are missing for such long time intervals. Here, for the first time, numerical tidal model simulations linked to climate model output are conducted for a range of paleogeographic configurations over the last 252 My. We find that the present is a poor guide to the past in terms of tidal dissipation: the total dissipation rates for most of the past 252 My were far below present levels. This allows us to quantify the reduced tidal dissipation rates over the most recent fraction of lunar history, and the lower dissipation allow refinement of orbitally-derived age models by inserting a complete additional precession cycle.

Keywords: tides, tidal drag, Earth-Moon evolution, Mesozoic-Cenozoic; numerical tidal model

*Corresponding author: E-mail: m.green@bangor.ac.uk

1. Introduction

Tidally induced energy dissipation in the earth and ocean gradually slows the Earth's rotation rate, changes Earth and lunar orbital parameters, and increases the Earth-Moon separation (Darwin, 1899; Munk, 1968). A long-standing conundrum exists in the evolution of the Earth-Moon system relating to the present recession rate of the moon and its age: if present day observed dissipation rates are representative of the past, the moon must be younger than 1500 Ma (Hansen, 1982; Sonett, 1996). This does not fit the age model of the solar system, putting the age of the moon around 4500 Ma (Hansen, 1982; Sonett, 1996; Walker and Zahnle, 1986; Canup and Asphaug, 2001; Waltham, 2004), and the possibility that the tidal dissipation rates have changed significantly over long time periods has been proposed (Hansen, 1982; Ooe, 1989; Poliakov, 2005; Green and Huber, 2013; Williams et al., 2014). A weaker tidal dissipation must be associated with a lower recession rate of the moon. Consequently, it can be argued that prolonged periods of weak tidal dissipation must have existed in the past (Webb, 1982; Bills and Ray, 1999; Williams, 2000). There is support for this in the literature using quite coarse resolution simulations driven by highly stylized, rather than historically accurate, boundary conditions (Munk, 1968; Kagan and Sundermann, 1996). However, with the present knowledge of the sensitivity of tidal models to resolution and boundary conditions, e.g., the oceans density structure (Egbert et al., 2004), the results of prior work should be revisited with state-of-the-art knowledge and numerical tools.

It was recently shown through numerical tidal model simulations with higher resolution than in previous studies that the tidal dissipation during the early Eocene (50 Ma) was just under half of that at present (Green and Huber, 2013). This is in stark contrast to the Last Glacial Maximum (LGM, around 20 ka) when simulated tidal dissipation rates were significantly higher than at present due to changes in the resonant properties of the ocean (Green, 2010; Wilmes and Green, 2014; Schmittner et al., 2015). However, the surprisingly large tides during the LGM are due to a quite specific combination of continental scale

31 bathymetry and low sea-level, in which the Atlantic is close to resonance when
 32 the continental shelf seas were exposed due to the formation of extensive conti-
 33 nental ice sheets (Platzman et al., 1981; Egbert et al., 2004; Green, 2010). It is
 34 therefore reasonable to assume — and proxies support this — that the Earth has
 35 only experienced very large tides during the glacial cycles over the last 1–2 Ma
 36 and that the rates have been lower than at present during the Cenozoic (Palike
 37 and Shackleton, 2000; Lourens and Brumsack, 2001; Lourens and et al., 2001).
 38 Such (generally) low tidal dissipation rates may have led to reduced levels of
 39 ocean mixing, with potential consequences for the large scale ocean circulation,
 40 including the Meridional Overturning Circulation (Munk, 1966; Wunsch and
 41 Ferrari, 2004).

42 The tidally induced lunar recession and increased day length also act to re-
 43 duce the precession rate of Earth’s axis and, as a result, produce falling rates of
 44 climatic precession and obliquity oscillation through time (Berger et al., 1992).
 45 As a direct consequence, cyclostratigraphy may be severely compromised be-
 46 cause many important Milankovitch cycle periods are directly affected by Earth-
 47 Moon separation. Nevertheless, Milankovitch frequencies have been estimated
 48 assuming either a constant lunar-recession rate or a constant tidal dissipation
 49 rate (Berger et al., 1992; Laskar et al., 2004). Based on the literature related to
 50 tidal evolution mentioned above, neither assumption is valid. For example, it
 51 was recently suggested that the tidal dissipation between 11.5–12.3 Ma was ei-
 52 ther at least 90% of the Present Day (PD) rate or 40% of the present rate, with
 53 the lower estimate obtained by shifting the precession a whole cycle (Zeeden
 54 et al., 2014). Constraining the tidal dissipation rates on geological time scales is
 55 consequently important. Investigating the tidal dynamics for select time slices
 56 over the Cenozoic era will shed light on the changes of tidal dissipation and
 57 hence on Earth-Moon system evolution.

58 Our aim in this paper is to answer the basic question: when considering the
 59 past, should our null hypothesis be that tidal dissipation was near modern values
 60 (the most common approach), much higher (suggested by LGM), or much lower
 61 (such as found for the Eocene)? We use the same tidal model as Green and

Huber (2013) and we present results from simulations of the tidal dynamics for the PD, LGM (21ka, Green, 2010), Pliocene (3 Ma), Miocene (25 Ma), Eocene (50 Ma, Green and Huber, 2013), Cretaceous (114 Ma, Wells et al., 2010), and for the Permian-Triassic (252 Ma). We explore dissipation changes across a wide cross-section of ocean states and paleogeographic configurations, from the nearly modern to a world with one global ocean basin, and we investigate sensitivity to substantial imposed changes in ocean stratification. Consequently, this encompasses the likely range of continental and paleoclimate configurations over much of Earth’s history.

2. Methods

2.1. Tidal modelling

The simulations of the global tides were done using the Oregon State University Tidal Inversion Software (OTIS Egbert et al., 1994). OTIS has been used in several previous investigations to simulate global tides in the past and present oceans (Egbert et al., 2004; Green, 2010; Green and Huber, 2013; Wilmes and Green, 2014). It provides a numerical solution to the linearized shallow water equations,

$$\frac{\partial \mathbf{U}}{\partial t} + \mathbf{f} \times \mathbf{U} = -gH\nabla(\eta - \eta_{SAL} - \eta_{EQ}) - \mathbf{F} \quad (1)$$

$$\frac{\partial \eta}{\partial t} - \nabla \cdot \mathbf{U} = 0 \quad (2)$$

Here $U = uH$ is the volume transport given by the velocity u multiplied by the water depth H , f is the Coriolis parameter, η the tidal elevation, η_{SAL} the self-attraction and loading elevation, η_{EQ} the equilibrium tidal elevation, and \mathbf{F} the dissipative term. Self-attraction and loading was introduced by doing 5 iterations following the methodology in Egbert et al. (2004). The dissipative term is split into two parts: $\mathbf{F} = \mathbf{F}_B + \mathbf{F}_W$. The first of these represents bed friction and is written as

$$\mathbf{F}_B = C_d \mathbf{u} |\mathbf{u}| \quad (3)$$

86 where C_d is a drag coefficient, and \mathbf{u} is the total velocity vector for all the tidal
 87 constituents. We used $C_d = 0.003$ in the simulations described below, but for
 88 all time slices simulations were done where C_d was increased or decreased by a
 89 factor 3 to estimate the sensitivity of the model to bed roughness. This only
 90 introduced minor changes in the results (within a few percent of the control),
 91 and we opted to use the value which provided the best fit to observations for
 92 the present. The second part of the dissipative term, $\mathbf{F}_w = C\mathbf{U}$, is a vector
 93 describing energy losses due to tidal conversion. The conversion coefficient C is
 94 here defined as (Green and Huber, 2013)

$$C(x, y) = \gamma \frac{(\nabla H)^2 N_b \bar{N}}{8\pi\omega} \quad (4)$$

95 in which $\gamma = 100$ is a scaling factor, N_b is the buoyancy frequency at the sea-
 96 bed (taken from coupled climate model outputs), \bar{N} is the vertical average of
 97 the buoyancy frequency, and ω is the frequency of the tidal constituent under
 98 evaluation. We did simulations with varying scaling factors (with $50 < \gamma < 200$)
 99 to cover the possible ranges of N , with only minor quantitative changes to
 100 the overall dissipation rates. This means that errors and uncertainties in the
 101 estimates of the buoyancy frequency from the climate model simulations will
 102 only change the quantitative results less than 10%.

103 The PD bathymetry is a combination of v.14 of the Smith and Sandwell
 104 database (Smith and Sandwell, 1997) with data for the Arctic (Jakobsson et al.,
 105 2012), northwards of 79°N, and Antarctic (Padman et al., 2002), southwards of
 106 79°S. All data were then averaged to 1/4° in both latitude and longitude.

107 The PD control simulation is compared to the TPXO8 database, an inverse
 108 tidal solution for both elevation and velocity based on satellite altimetry and the
 109 shallow water equations (see Egbert and Erofeeva, 2002, and [http://volkov.oce.](http://volkov.oce.orst.edu/tides/tpxo8_atlas.html)
 110 [orst.edu/tides/tpxo8_atlas.html](http://volkov.oce.orst.edu/tides/tpxo8_atlas.html) for details). The root-mean-square (RMS)
 111 difference between the modeled and observed elevations is computed, along
 112 with the percentage of sea surface elevation variance captured, given by $V =$
 113 $100[1 - (S/RMS)^2]$, where RMS is the RMS discrepancy between the modeled
 114 elevations and the TPXO elevations, and S is the RMS of the TPXO elevations.

115 The tidal dissipation, D , is computed using (Egbert and Ray, 2001):

$$D = W - \nabla \cdot P \quad (5)$$

116 in which W is the work done by the tide-producing force and P is the energy
117 flux. They are defined as

$$W = g\rho\langle \mathbf{U} \cdot \nabla (\eta_{SAL} + \eta_{EQ}) \rangle \quad (6)$$

$$P = g\rho\langle \eta \mathbf{U} \rangle \quad (7)$$

118 in which the angular brackets mark time-averages. When we discuss the accu-
119 racy and the energy dissipation rates we use a cutoff between deep and shallow
120 water at 1000 m depth.

121 2.2. Earth-moon separation

122 The tidal dissipation rate, D , should be (Murray and Dermott, 2010)

$$D = 0.5m'na(\Omega - n)\frac{\partial a}{\partial t} \quad (8)$$

123 where $m' = mM/(m + M)$, m is Moon-mass, M is Earth-mass, a is the Earth-
124 Moon separation, Ω is the Earth's rotation rate and n is the lunar mean motion.
125 The next step is to note that lunar recession is well approximated using (Lam-
126 beck, 1980; Bills and Ray, 1999; Waltham, 2015)

$$\frac{\partial a}{\partial t} = fa^{-5.5} \quad (9)$$

127 where the tidal drag factor

$$f = 3\frac{k_2m}{QM}R^5\sqrt{\mu} \quad (10)$$

128 In which k_2 is Earth's Love number, Q is the tidal quality factor, R is Earth's
129 radius whilst, from Kepler's 3rd Law

$$\mu = G(m + M) = n^2a^3 \quad (11)$$

130 Combining Eqs. (8)–(11) yields

$$f = \frac{2Da^6}{m'\sqrt{\mu}(\Omega - n)} \quad (12)$$

131 Note that the tidal dissipation rates calculated in Table 1 assumed the present-
 132 day day-length and Earth-Moon separation. All terms in Eq. (12), except P,
 133 were therefore constant so $f/f_{PD} = D/D_{PD}$. This is a reasonable approxima-
 134 tion as day-lengths and Earth-Moon separation only change by a few percent
 135 over the time-range considered (e.g., Waltham, 2015).

136 3. Results

137 3.1. Tidal evolution

138 Simulations were carried out with the M_2 , S_2 , K_1 , and O_1 tidal constituents
 139 included (representing the principle lunar and solar semidiurnal constituents,

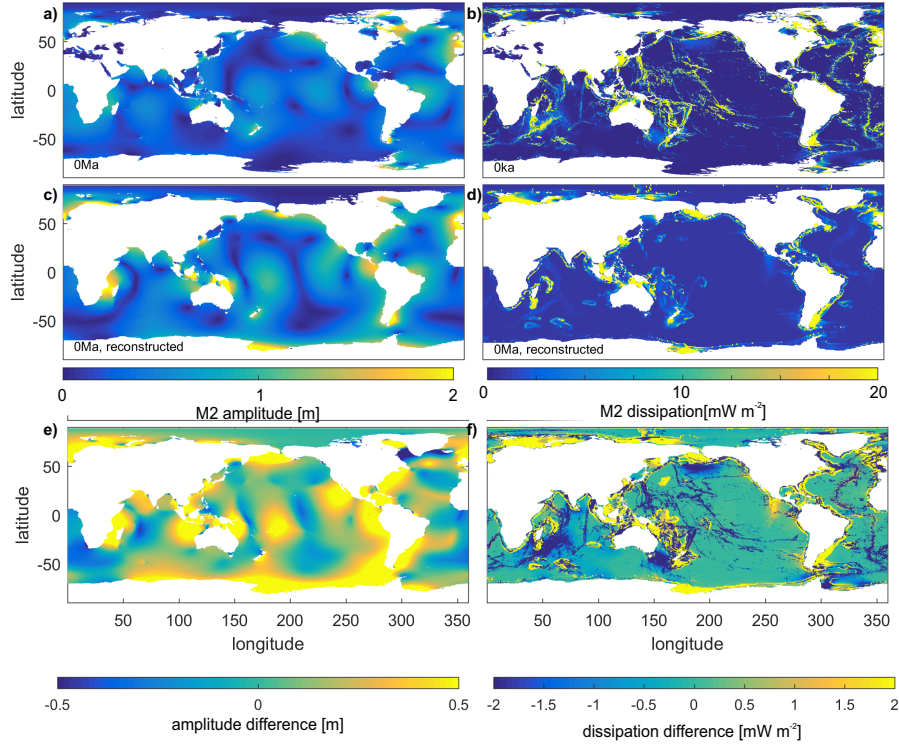


Figure 1: Modelled M_2 tidal amplitudes for the PD (a) and the PD reconstruction (c), and the difference between the two panels (e). Panels b, d, and f show the tidal dissipation rates associated with the amplitudes.

Table 1: The integrated tidal dissipation rates (in TW) for the M_2 constituent for the global (“total”) and abyssal (“deep”, i.e., deeper than 1000 m) ocean. The relative rate for PD is normalised with the PD reconstructed rate, whereas the relative LGM rate is normalised with the PD rate (see Figure 1 and the text for a discussion).

Period, Age	absolute		relative	Comment/source
	total	deep	total	
PD	2.8	0.9	0.62	Green and Huber (2013)
PD reconstructed	4.5	1.0	1	PD with reconstructed bathymetry
LGM 0.021 Ma	4.0	1.5	1.42	Wilmes and Green (2014), relative to PD

140 and constituents representing the diurnal luni-solar and lunar declinations, re-
 141 spectively). Here, we limit our discussion to M_2 as changes in the other con-
 142 stituents are similar to those in M_2 but smaller in magnitude (see the discussion
 143 below). Building on prior work we aim to create a time history of paleodissipa-
 144 tion by filling in new simulations of the Permian-Triassic, Cretaceous, Miocene,
 145 and Pliocene. To further understand the sensitivity of our results to our method-
 146 ological choices and to establish their robustness we conducted a degraded PD
 147 sensitivity simulation, in which we used a bathymetric database for the present
 148 ocean derived using the same geophysical principals and methods as our paleo-
 149 bathymetries (see Matthews et al., 2015). This simulation showed a total M_2
 150 dissipation of some 4.5 TW, of which 1 TW dissipated in deep waters (Table 1
 151 and Figure 1). This is within a factor 2 of our values using present day observed
 152 bathymetry (2.8 TW in total and 0.9 TW in the deep, respectively) and leads
 153 us to conclude that we most likely overestimate the dissipation rates in our
 154 paleo-simulations due to a lack of abyssal topography (see Egbert et al., 2004,
 155 for a similar discussion). Our integrated values presented below are therefore
 156 probably on the high side in terms of absolute magnitude but we concentrate on
 157 relative changes in this study. The robustness of our results in our sensitivity
 158 simulation also gives us confidence in our bathymetric databases. In the rest
 159 of this analysis we generally present results normalized by the reconstructed
 160 PD dissipation values in order to show only relative changes with respect to the

Table 2: The integrated absolute tidal dissipation rates (in TW) for the M_2 constituent for the palaeo-simulations. Shown are again data for the global (“total”) and abyssal (“deep”, i.e., deeper than 1000 m) ocean. The relative rate is normalised with the total rate for the reconstructed PD simulation.

Period, Age	absolute		relative	Comment/source
	total	deep	total	
Pliocene 3 Ma	2.4	0.6	0.53	
Miocene 25Ma	2.2	0.6	0.49	
	1.9	1.7	0.43	PD bathymetry, Miocene stratification
	3.3	<0.1	0.73	PD stratification, Miocene bathymetry
Eocene 50 Ma	1.4	1.2	0.32	Green and Huber (2013)
	1.4	1.2	0.32	CO ₂ = 240 ppm
	1.4	1.2	0.32	CO ₂ = 560 ppm
	1.4	1.2	0.32	CO ₂ = 1120 ppm
	1.4	1.2	0.32	Tasman Gateway open
	1.4	1.2	0.32	Drake Passage open
Cretaceous 116Ma	2.1	1.3	0.47	
	2.0	1.5	0.44	Tidal conversion x2
	2.1	1.0	0.47	Tidal conversion x0.5
Permian-Triassic 252 Ma	0.9	0.1	0.2	
	0.8	0.2	0.18	Tidal conversion x2

modern degraded simulation. The one exception is the LGM study, which is normalized by the undegraded PD simulations since modern observed bathymetry was used in this simulation. In the following we refer the reader to Figure 1 and Table 1 for the PD results, and Figures 2–3 for palaeo-tidal M_2 amplitudes and dissipation rates, respectively. Table 2 and Figure 4 summarise the globally integrated relative dissipation rates.

The Pliocene simulations exhibit a reduced amplitude and subsequent dissipation rate (53%) compared to the degraded PD tides, but with a very similar distribution (Figures 2b and 3b). This is due to sea-level being some 25m higher

170 than at present during this period and is consistent with previously reported
 171 simulations with extreme sea level rise (SLR; Green and Huber, 2013). The dy-
 172 namical explanation is that the large SLR cause global dissipation rates to drop
 173 below present because the near-resonant North Atlantic experiences decreased
 174 dissipation rates with SLR due to larger shelf seas (Green, 2010).

175 Simulated Miocene tides resemble the modeled degraded PD tides to some
 176 extent, but they are generally weaker than at present (Figures 2c and 3c). The
 177 globally integrated dissipation rate for the Miocene is 2.2 TW, or 50% of the de-
 178 graded model present rate. These changes are mainly explained by the Atlantic
 179 being narrower during the Miocene than the PD. The North Atlantic is therefore
 180 no longer near resonance for the semi-diurnal tide, which reduces the simulated

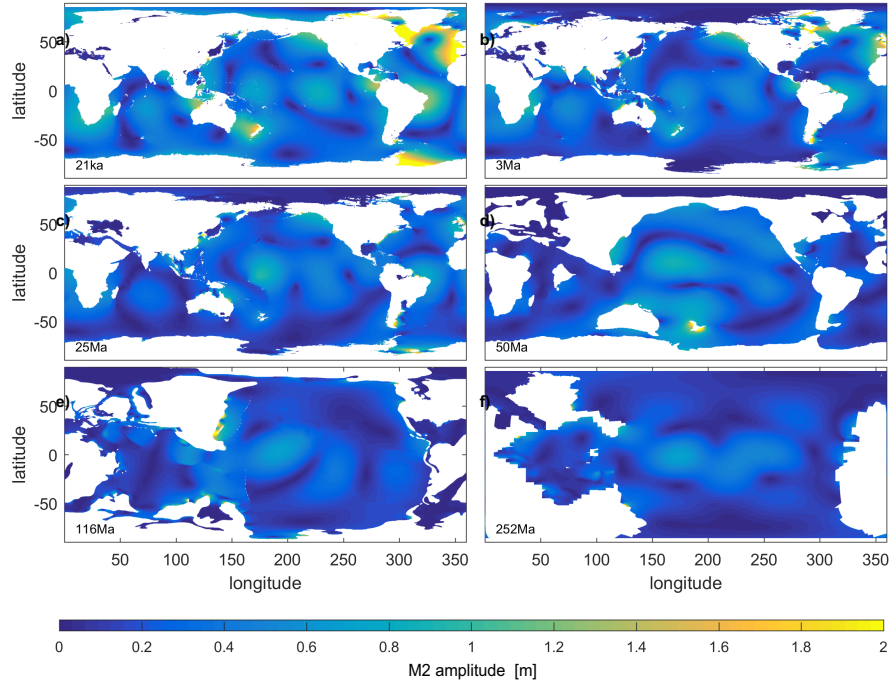


Figure 2: Shown are the M_2 tidal amplitudes for the LGM (a), Pliocene (b), Miocene (c), Eocene (d), Cretaceous (e) and Permian-Triassic (f).

181 Miocene tidal amplitudes. The vertical stratification in our Miocene simulations
 182 was stronger than at present due to different ocean gateway configurations and
 183 the lack of North Atlantic Deepwater formation, which leads to a more stably
 184 stratified ocean (Herold et al., 2012). This enhances the tidal conversion in the
 185 abyssal ocean, and as a consequence there is more energy being lost in the deep
 186 ocean in the Miocene case than at present. Further support comes from sensi-
 187 tivity simulations which used enhanced or reduced stratifications based on the
 188 ratio between the averaged PD and Miocene buoyancy frequencies (not shown).
 189 In these runs a combination of Miocene stratification and PD bathymetry leads
 190 to a reduced global and enhanced abyssal dissipation compared to the Miocene
 191 control simulation. The opposite holds when using PD stratification with the

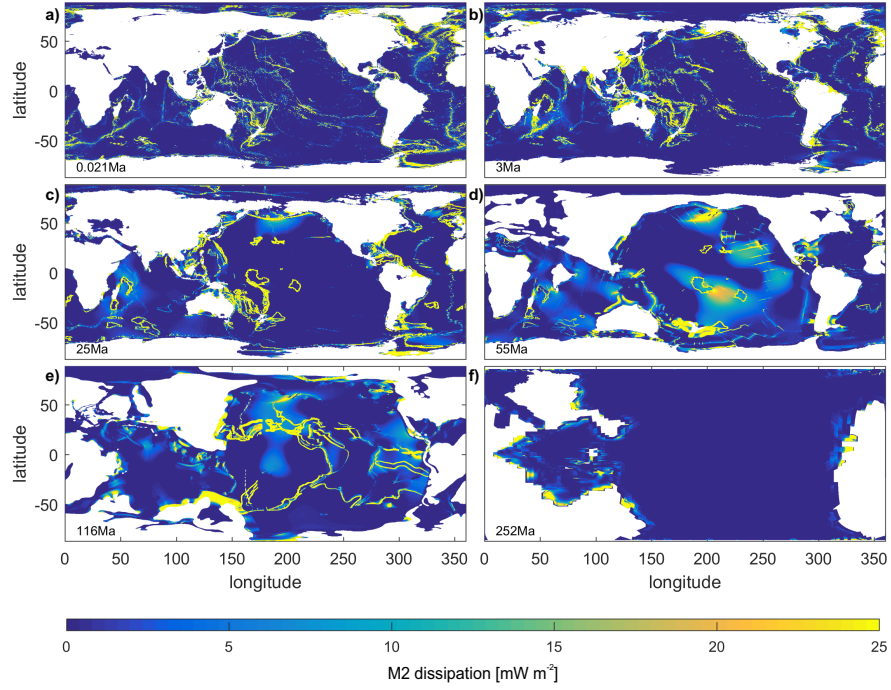


Figure 3: As in Figure 2, but showing the modelled *absolute* tidal dissipation rates.

192 Miocene bathymetry.

193 We have carried out a set of climate model sensitivity runs to complement
 194 the earlier Eocene simulation (see Table 2). These used a tidally driven dif-
 195 fusivity parameterization (Green and Huber, 2013) but with atmospheric CO₂
 196 concentrations of 240 ppm, 560 ppm, and 1120 ppm. Further runs with Drake
 197 Passage or the Tasman Gateway open were also conducted, using 560 ppmCO₂
 198 (changes in CO₂ may affect tides by modifying the stratification-dependent tidal
 199 conversion rate). These simulations were carried out to bound the sensitivity
 200 of the Eocene results to likely changes in surface climate and ocean gateway
 201 configuration that are thought to have altered ocean stratification, a key pa-
 202 rameter in tidal studies. There are only small changes in the tidal conversion
 203 rates between these runs and the Eocene control (see our Table 2, Figures 2d
 204 and 3, and Green and Huber, 2013), indicating that the ocean state and tidal
 205 dissipation are convergent.

206 The new model results for the Cretaceous show a somewhat energetic ocean,
 207 dissipating nearly as much energy as the Miocene (Figures 2e and 3e). The rea-
 208 son for this quite large simulated dissipation rate lies in the rifting of Gondwana-
 209 land, which generated extensive new coastlines and a corresponding increase in
 210 the surface area of shallow shelf seas (Wells et al., 2010). The Cretaceous shelf

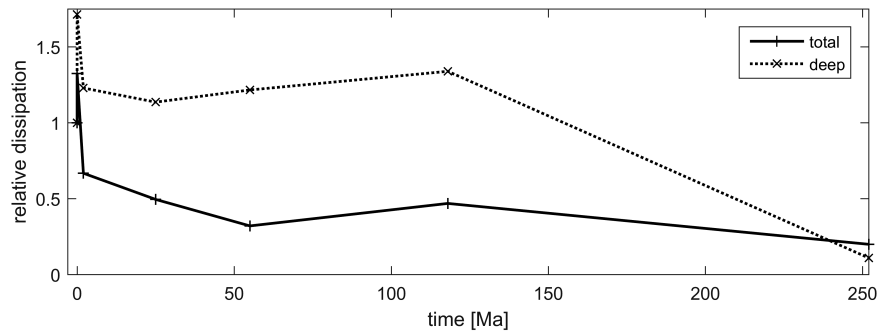


Figure 4: Shown are the *relative* dissipation rates, normalized with the results from the PD sensitivity run. This confirms that total rates have been lower over the last 252Ma, but that the abyssal rates have generally been larger than today.

211 seas in the model cover an area more than three times larger than that at
 212 present. These very vast shallow areas, together with a strong vertical stratifi-
 213 cation (the average buoyancy frequency used in the model is nearly twice that at
 214 Present, e.g., Zhou et al., 2012; Poulsen and Zhou, 2013; Domeier, 2016), lead to
 215 relatively large dissipation rates overall. A large fraction of this energy, about
 216 62%, ends up in the deep ocean in the simulations. The lack of knowledge about
 217 the abyssal topography for this period can be compensated for by varying the
 218 tidal conversion coefficient as a sensitivity parameter. Using factors of 0.5 and
 219 2 above the already doubled value compared to PD discussed above to provide
 220 sensitivity estimates, we still obtain much less than modern dissipation in the
 221 Cretaceous case (Table 2) and are confident in our conclusions.

222 The Permian-Triassic (PT) simulations show very weak tides with a dissipa-
 223 tion in total of about 1 TW (22% of degraded PD; (Figures 2f and 3f) — 10%
 224 of which dissipates in the deep ocean. These results are readily understandable,
 225 as the large recent dissipation rates are an effect of complex bathymetry and
 226 local resonances in smaller basins between continents and such features were
 227 absent during the PT (see Muller et al., 2016, for a discussion). Simulations of
 228 a PD water world show similar behaviour, albeit with even weaker tides than we
 229 find here, because with less topographic variations we approach the theoretical
 230 equilibrium tide (Arbic et al., 2009). The PT simulation with a doubled tidal
 231 conversion coefficient, representing unaccounted for topographic roughness (see
 232 Table 2), showed a 45% increase in the abyssal rates but a 9% reduction in total
 233 dissipation. This again puts us on the safe side with our conclusions because
 234 we probably overestimate the dissipation slightly in the PT control run.

235 The horizontally integrated dissipation rates for the other constituents, S_2 ,
 236 K_1 and O_1 , are shown in Figure 5. It is evident from Figure 5 that the behaviour
 237 of these constituents mimic that of the M_2 tide and that the M_2 is a good
 238 representation of the global tidal dissipation. It is possible that basins may
 239 become resonant for the diurnal constituents (although this has not been spotted
 240 in our simulations), but they are by their very nature less energetic than M_2 .
 241 The conversion of energy in the diurnal constituents is also more restricted due

242 to the critical latitude being only 30° (see Falahat and Nycander, 2015, for a
 243 discussion).

244 3.2. Consequences for the Earth-Moon system

245 The lower-than-modern tidal dissipation rates simulated through the Ceno-
 246 zoic and Mesozoic shows that the lunar recession rate was probably smaller than
 247 otherwise predicted in the past. The questions raised are i) by how much? and
 248 ii) how did this impact on the lunar distance? Using the recession model in
 249 Section 2.2, we show that the relative tidal dissipations in Table 1–2 are also
 250 the relative tidal-drag ratios. It is notable that all but the most recent ratios
 251 are significantly below unity. This is consistent, however, with the observation
 252 that the long-term mean drag must be around $f/f_{PD} = 0.33 \pm 0.03$ if the Moon-
 253 forming collision occurred at 4500 ± 50 Ma (Waltham, 2015). The implications

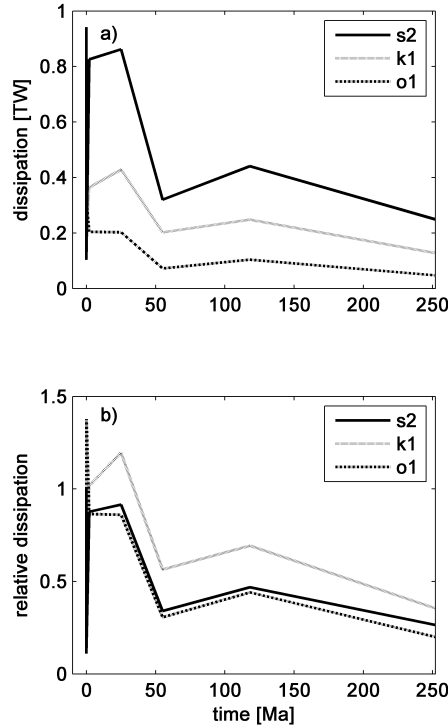


Figure 5: As in Figure 4 but for the S_2 , K_1 , and O_1 constituents.

254 of both the ancient origin of our Moon, and the tidal-dissipation modelling in
 255 this paper, are that present day tidal dissipation is anomalously high. Given
 256 the results in Table 2, the typical tidal drag over the last 250 Ma is $f/f_{PD} =$
 257 0.63 ± 0.16 (1 standard error). Using this result in Eq. (9) then yields the Earth-
 258 Moon separation history shown in Figure 6. For comparison, Figure 6 also shows
 259 the results of full numerical modelling by Laskar et al. (2004) along with the
 260 results of using Eq. (9) assuming $f/f_{PD} = 1$. Note that Laskar et al. (2004)
 261 assumed that tidal lag (which is closely related to tidal drag) did not vary from
 262 the present day value in the past.

263 4. Discussion

264 It is obvious, especially from the sensitivity tidal simulations, that the lunar
 265 distance would have been changing more slowly in the past than would be pre-
 266 dicted assuming modern dissipation rates. It has been suggested that the aver-
 267 age recession rate from the late Neoproterozoic (620 Ma) to PD is 2.17 cm yr^{-1} ,
 268 and that the recession rate during the Proterozoic (2450–620 Ma) cannot have
 269 exceeded of 1.24 cm yr^{-1} (Williams, 2000). Both of these statements are sup-
 270 ported here, and we suggest that the rates may even have been lower. Fur-

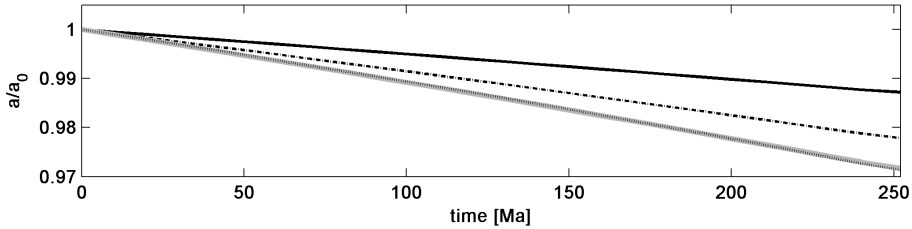


Figure 6: Earth-Moon separation through time from Equations (9)–(12). The solid and dashed-dotted black lines show the range assuming the tidal-dissipation range of this paper. The solid grey line shows lunar-recession assuming that tidal-dissipation equalled the present day dissipation in the past, whereas the black dotted line shows the lunar-separation history predicted by the full numerical model from Laskar et al. (2004). Note that the Laskar model is virtually identical to our curve, assuming PD tidal drag, but that the lower mean-drag shown in this paper gives a reduced separation in the past.

thermore, because the recession rate is proportional to tidal-lag (Laskar et al., 2004) and we have shown that the recession rate is proportional to dissipation, the tidal-lag must have an uncertainty of a factor of 2 or more. This confirms, using a very different approach, suggestions about uncertainty in Milankovitch periods and cyclostratigraphy (Waltham, 2015). Furthermore, sensitivity simulations (not shown) with sea-level being 80m higher or lower in each time slice did not significantly change the results, except for PD, when large shelf seas are present and allowed to dry out or flood further (see Green and Huber, 2013, for a discussion). From these results it also appears that Earth is near a tidal maximum at present, although full glacial conditions enhance dissipation by a further 42%.

Given that most of the Phanerozoic has been spent with either much warmer climate than modern conditions (with weaker stratification) or continents more widely spaced and oceans out of resonance, it is now clear that the modern situation is a poor guide to the past as suggested by Hansen (1982). A more accurate null hypothesis is to assume that overall tidal dissipation was typically $\approx 50\%$ of modern values, although subject to significant variation. Interestingly, this result compares well with independent estimates from rhythmites (Williams, 2000; Coughenour et al., 2013). The similarity of the results obtained here with prior modeling work utilizing much simpler physical formulations of dissipation and much cruder representations of varying boundary conditions (Hansen, 1982; Webb, 1982; Kagan and Sundermann, 1996; Poliakov, 2005) is also noteworthy. This similarity confirms that the physics of tidal dissipation and the bulk variables that cause it to vary are robust and constrainable.

Tides are of course not the only process affecting orbital parameters, and the different plate tectonic configurations over the past 252 Ma may have altered the dynamical ellipticity, adding to the changes discussed here. This is, as stated in the introduction, an investigation into how the tides may have changed over long geological time scales and the possible contributions from the tides. Other mechanisms are left to other investigations. The ability to put significant bounds on tidal dissipation through time has substantial implications, espe-

302 cially for improving knowledge of Earth’s precession parameters through time.
 303 The combination of tidal dissipation and the dynamical ellipticity (or so-called
 304 precession constant) is crucial for gaining more accurate solutions to Earth’s
 305 precession and obliquity behaviours on long time scales. The importance of dis-
 306 sipation and dynamical ellipticity to these precession parameters allows them to
 307 be inferred by inverting interference patterns between obliquity and precession
 308 bands derived from long paleoclimate time-series and comparison with orbital
 309 calculations. From these calculations constraints on the summed behaviour of
 310 tidal dissipation and dynamical ellipticity can be gained, although the solutions
 311 tend to be non-unique. It has been suggested that a tidal dissipation value of
 312 approximately half of the modern rate characterized the past 3 Ma well (Lourens
 313 and Brumsack, 2001). This is in agreement with our results, but that study did
 314 not explore sensitivity to dynamical ellipticity. Significant uncertainty remains
 315 on this issue; other studies have reached the conclusion that tidal dissipation
 316 may have been higher (Palike and Shackleton, 2000), whereas more recent work,
 317 extending these methods further back to the early Miocene, show as much ev-
 318 idence for low (30–50% of modern) values of dissipation as they do higher (by
 319 20%)(Husing et al., 2007; Zeeden et al., 2014). What is clear however, is that
 320 integrating these various approaches, including explicit modelling of tidal dis-
 321 sipation, will help resolve important paleoclimate and geophysical enigmas and
 322 improve cyclostratigraphic age models. For example, our low dissipation rates
 323 in Figure 3 agree with the lower range of dissipation values from Zeeden et al.
 324 (2014) for 11.5–12.3 Ma if we shift the orbitally derived time scale for this inter-
 325 val by a whole precession cycle as compared to using a modern value. Explicitly
 326 modelling tidal dissipation will enable one of the two key free parameters in pre-
 327 cession and obliquity calculations to be constrained which will enable a better
 328 understanding of the factors determining dynamical ellipticity.

329 The weaker tidally induced ocean mixing during the Phanerozoic may also
 330 have influenced the Meridional Overturning Circulation, with potential conse-
 331 quences for climate. Green and Huber (2013) used modelled stratification for
 332 the Eocene, whereas Schmittner et al. (2015) simulated the LGM with modelled

stratification. Both investigations highlight local changes in dissipation, but the overall rates stayed within the range given by our sensitivity simulations. However, the percentage of upwelling from the deep was sometimes greater than at Present, and the consequences for the ocean circulation of reduced (tidally driven) mixing is complex and needs further investigation.

5. Conclusions

Results from an established numerical tidal model suggest that the tidal dissipation during the Cenozoic and Late Cretaceous were weaker than at present, with the exception of the glacial states over the last 2Ma. It is very likely that the Earth-Moon system is unusually dissipative at present. Consequently, the Moon’s recession rate was slower in the deep past than predicted using PD dissipation rates, supporting the old-age Earth-Moon model. Furthermore, our relative dissipation rates in Figure4 support the lower range of dissipation values from Zeeden et al. (2014), who claim that the tidal dissipation between 11.5–12.3 Ma was either within 10% of PD values or 40% of the present rate. This has significant implications for climate proxy reconstructions: their lower estimate of the tidal dissipation rate was obtained by inserting a complete additional precession cycle, which our relative rates show is the correct dissipation rate to use. This highlights the importance of dynamic ellipticity in orbital chronology calculations, and it shows that accurate tidal dissipation rates must be used in investigations of palaeo-climates.

Acknowledgements: The tidal simulation output is available from the corresponding author. Funding was provided by the Natural Environmental Research Council (grants NE/F014821/1 and NE/I030224/1 to JAMG), and the National Science Foundation (grant 0927946-ATM to MH). Simulations were done using HPCWales, and technical support from Ade Fewings is gratefully acknowledged.

Arbic, B. K., Karsten, R. H., Garrett, C., 2009. On tidal resonance in the global ocean and the back-effect of coastal tides upon open-ocean tides. *Atmosphere-Ocean* 47, 239–266.

362 Berger, A., Loutre, M., Laskar, J., 1992. Stability of the astronomical frequencies
363 of the earth's history for paleoclimate studies. *Science* 255, 560–566.

364 Bills, B., Ray, R., 1999. Lunar orbital evolution: A synthesis of recent results.
365 *Geophysical Research Letters* 26, 3045–3048.

366 Canup, R., Asphaug, E., 2001. Origin of the moon in a giant impact near the
367 end of the earth's formation. *Nature* 412, 708–712.

368 Coughenour, C., Archer, A., Lacovara, K., 2013. Calculating earth-moon sys-
369 tem parameters from sub-yearly tidal deposit records: an example from the
370 carboniferous tradewater formation. *Sedimentary Geology* 295, 67–76.

371 Darwin, G. H., 1899. The tides and kindred phenomena in the solar system.
372 Houghton, Boston.

373 Domeier, M., 2016. Vegetation-climate interactions in the warm mid-Cretaceous.
374 *Gondwana Research* 36, 275–295.

375 Egbert, G. D., Bennet, A. F., Foreman, M. G. G., 1994. Topex/Poseidon tides
376 estimated using a global inverse model. *Journal of Geophysical Research* 99,
377 24821–24852.

378 Egbert, G. D., Bills, B. G., Ray, R. D., 2004. Numerical modeling of the global
379 semidiurnal tide in the present day and in the last glacial maximum. *Journal*
380 *of Geophysical Research* 109, C03003, doi: 10.1029/2003JC001973.

381 Egbert, G. D., Erofeeva, S., 2002. Efficient inverse modeling of barotropic ocean
382 tides. *Journal of Atmospheric and Oceanic Technology* 19, 183–204.

383 Egbert, G. D., Ray, R. D., 2001. Estimates of M2 tidal energy dissipation from
384 Topex/Poseidon altimeter data. *Journal of Geophysical Research* 106, 22475–
385 22502.

386 Falahat, S., Nycander, J., 2015. On the generation of bottom-trapped internal
387 tides. *Journal of Physical Oceanography* 42, 526–545.

388 Green, J. A. M., 2010. Ocean tides and resonance. *Ocean Dynamics* 60.

389 Green, J. A. M., Huber, M., 2013. Tidal dissipation in the early Eocene
390 and implications for ocean mixing. *Geophysical Research Letters* 40,
391 doi:10.1002/grl.50510.

392 Hansen, K., 1982. Secular effects of oceanic tidal dissipation on the moons orbit
393 and the earth's rotation. *Reviews of Geophysics* 20, 457–480.

394 Herold, N., Huber, M., M \tilde{A} $\frac{1}{4}$ ller, R. D., Seton, M., 2012. Modeling the miocene
395 climatic optimum: Ocean circulation. *Paleoceanography* 27, PA1209.

396 Husing, S., Hilgen, F., AbdulAziz, H., Krijgsman, W., 2007. Completing the
397 neogene geological time scale between 8.5 and 12.5 ma. *Earth and Planetary*
398 *Science Letters* 253, 340–358.

399 Jakobsson, M., Mayer, L. A., Coakley, B., Dowdeswell, J. A., Forbes, S., Frid-
400 man, B., Hodnesdal, H., Noormets, R., Pedersen, R., Rebesco, M., Schenke,
401 H.-W., A, Y. Z., Accettella, D., Armstrong, A., Anderson, R. M., Bienhoff,
402 P., Camerlenghi, A., Church, I., Edwards, M., Gardner, J. V., Hall, J. K.,
403 Hell, B., Hestvik, O. B., Kristoffersen, Y., Marcussen, C., Mohammad, R.,
404 Mosher, D., Nghiem, S. V., Pedrosa, M. T., Travaglini, P. G., Weatherall,
405 P., 2012. The International Bathymetric Chart of the Arctic Ocean (IBCAO)
406 Version 3.0. *Geophysical Research Letters* 10.1029/2012GL052219.

407 Kagan, B., Sundermann, A., 1996. Dissipation of tidal energy, paleotides, and
408 evolution of the earth-moon system. *Advances in Geophysics* 38, 179–266.

409 Lambeck, K., 1980. The earth's variable rotation: geophysical causes and con-
410 sequences. Cambridge University Press. Cambridge, UK.

411 Laskar, J., Robutel, P., Joutel, F., Correia, M. G. A., Levrard, B., 2004. A long-
412 term numerical solution for the insolation quantities of the earth. *Astronomy*
413 *and Astrophysics* 428, 261–285.

414 Lourens, L., Brumsack, R. W. H., 2001. Geological constraints on tidal dissipa-
 415 tion and dynamical ellipticity of the earth over the past three million years.
 416 Nature 409, 1029–1033.

417 Lourens, L., et al., 2001. Astronomical pacing of late palaeocene to early eocene
 418 global warming events. Nature 7045, 1083–1087.

419 Matthews, K., Williams, S., Whittaker, J., Muller, R., Seton, M., Clarke, G.,
 420 2015. Geologic and kinematic constraints on late cretaceous to mid eocene
 421 plate boundaries in the southwest pacific. Earth-Science Reviews 140, 72–
 422 107.

423 Muller, R. D., Seton, M., Zahirovic, S., Williams, S. E., Matthews, K. J., Wright,
 424 N. M., Shephard, G. E., Maloney, K. T., Barnett-Moore, N., Hosseinpour, M.,
 425 Bower, D. J., Cannon, J., 2016. Ocean basin evolution and global-scale plate
 426 reorganization events since Pangea breakup. Annual Reviews of Earth and
 427 Planetary Science 44, 107–138.

428 Munk, W., 1966. Abyssal recipes. Deep-Sea Research 13, 707–730.

429 Munk, W., 1968. Once again – tidal friction. Quarterly Journal of the Royal
 430 Astronomical Society 9, 352–375.

431 Murray, C., Dermott, S., 2010. Solar system dynamics. Cambridge University
 432 Press. 608pp.

433 Ooe, M., 1989. Effects of configuration and bathymetry of the oceans on the
 434 tidal dissipation of the earth’s rotation. Journal of Physics of the Earth 37,
 435 345–355.

436 Padman, L., Fricker, H. A., Coleman, R., Howard, S., Erofeeva, S., 2002. A new
 437 tidal model for the Antarctic ice shelves and seas. Annals of Glaciology 34,
 438 247–254.

439 Palike, H., Shackleton, N., 2000. Constraints on astronomical parameters from
 440 the geological record for the last 25 myr. Earth and Planetary Science Letters
 441 182, 1–14.

442 Platzman, G. W., Curtis, G. A., Hansen, K. S., Slater, R. D., 1981. Normal
 443 modes of the world ocean 2. description of modes in the periods range 8 to
 444 80 hours. *Journal of Physical Oceanography* 11, 579–603.

445 Poliakov, E., 2005. Numerical modelling of the paleotidal evolution of the earth-
 446 moon system. *Dynamics of populations of planetary systems* 197, 445–452.

447 Poulsen, C. J., Zhou, J., 2013. Sensitivity of Arctic climate variability to mean
 448 state: Insights from the Cretaceous. *Journal of Climate* 26, 7003–7022.

449 Schmittner, A., Green, J. A. M., Wilmes, S.-B., 2015. Glacial ocean overturning
 450 intensified by tidal mixing in a global circulation model. *Geophysical Research*
 451 *Letters* 42, doi:10.1002/2015GL0635610.

452 Smith, W. H. F., Sandwell, D. T., 1997. Global seafloor topography from satel-
 453 lite altimetry and ship depth soundings. *Science* 277, 1957–1962.

454 Sonett, C., 1996. Late proterozoic and paleozoic tides, retreat of the moon, and
 455 rotation of the earth. *Science* 273, 100–104.

456 Walker, J., Zahnle, K., 1986. Lunar nodal tide and distance to the moon during
 457 the precambrian. *Nature* 320, 600–602.

458 Waltham, D., 2004. Anthropoc selection for the moon’s mass. *Astrobiology* 4,
 459 460–468.

460 Waltham, D., 2015. Milankovitch period uncertainties and their impact on cy-
 461 clostratigraphy. *Journal of Sedimentary Research* 85, 990–998.

462 Webb, D., 1982. Tides and the evolution of the earth-moon system. *Geophysical*
 463 *Journal of the Royal Astronomical Society* 70, 261–271.

464 Wells, M., Allison, P., Piggott, M., Hampson, G., Pain, C., Gorman, G., 2010.
 465 Tidal modeling of an ancient tide-dominated seaway, part 1: model valida-
 466 tion and application to global early Cretaceous (Aptian) tides. *Journal of*
 467 *Sedimentary Research* 80, 393–410.

468 Williams, G., 2000. Geological constraints on the precambrian history of earth's
469 rotation and the moon's orbit. *Reviews of Geophysics* 38, 37–59.

470 Williams, J., Turyshv, S., Boggs, D., 2014. The past and present earth-moon
471 system: the speed of light stays steady as tides evolve. *Planetary Science* 3,
472 1–9.

473 Wilmes, S.-B., Green, J. A. M., 2014. The evolution of tides and tidally
474 driven mixing over 21,000 years. *Journal of Geophysical Research* 119,
475 doi:10.1002/2013JC009605.

476 Wunsch, C., Ferrari, R., 2004. Vertical mixing, energy, and the general circu-
477 lation of the oceans. *Annual Review of Fluid Mechanics* 36, 281–314, doi:10.
478 1146/annurev. fluid. 36. 050802. 122121.

479 Zeeden, C., Hilgen, F., Hüsing, S., Lourens, L., 2014. The miocene astronomical
480 time scale 9–12 ma: New constraints on tidal dissipation and their implica-
481 tions for paleoclimatic investigations. *Paleoceanography* 29, 296–307.

482 Zhou, J., Poulsen, C., Rosenbloom, N., Shields, C., Briegleb, B., 2012.
483 Vegetation-climate interactions in the warm mid-Cretaceous. *Climates of the*
484 *past* 8, 565–576.